Translational Oncology
www.transonc.com

Volume 2 Number 2 June 2009 pp. 96–106 96

Visualization and Quantification of Intraperitoneal Tumors by *In Vivo* Computed Tomography Using Negative Contrast Enhancement Strategy in a Mouse Model of Ovarian Cancer[1]

Murtuza Rampurwala*, Murali K. Ravoori†, Wei Wei‡, Valen E. Johnson‡, Raghunandan Vikram* and Vikas Kundra*,†

*Diagnostic Radiology, The University of Texas MD Anderson Cancer Center, Houston, TX, USA; †Department of Experimental Diagnostic Imaging, The University of Texas MD Anderson Cancer Center, Houston, TX, USA; ‡Department of Biostatistics, The University of Texas MD Anderson Cancer Center, Houston, TX, USA

Abstract

Small animal computed tomography (CT) has poor intrinsic soft tissue contrast, limiting evaluation of intra-abdominal structures. Using standard intravascular-extracellular intravenous contrast (IE-IV) alone is theoretically limited by long acquisition times of traditional small animal scanners that may result in equilibration. We assessed whether a negative contrast strategy of enhancing normal tissue surrounding tumor, instead of the tumor itself, can visualize and quantify intraperitoneal (IP) cancer in a mouse model. Two and a half weeks after IP injection of Hey A8 cells, four groups of three animals each were administered serial dilutions of IV Fenestra LC (RES-IV), oral Gastroview, and IP Optiray 320. Another group of three animals was administered IV Optiray 320 (IE-IV), oral Gastroview, and IP Optiray 320 in successive combinations. Both groups were imaged by CT. Tumor and organ Hounsfield units were measured, and visualization was assessed. With increasing contrast amount, the Hounsfield unit of organs generally increased, whereas that of tumor remained essentially stable. The visualization of abdominal organs and tumor also generally increased with increasing contrast amount. Visualization of tumor and its margins adjacent to liver, spleen, and stomach was significantly better on administering RES-IV. However, for tumor adjacent to bladder, both IE-IV and RES-IV were equivalent. *In vivo* CT-derived tumor weights correlated highly with *ex vivo* tumor weights ($r = 0.96$, $P < .0001$, $n = 15$). Thus, CT using negative contrast enhancement strategy allows visualization and quantification of IP tumors. Such a strategy will also enable anatomic localization of functional signal for combination/molecular imaging.

Translational Oncology (2009) 2, 96–106

Introduction

Of 58 women, 1 will develop ovarian cancer during her lifetime [1]. It is the most common cause of death from gynecologic malignancy, and overall, the fifth most common cause of cancer death in women [2]. An estimated 22,430 new cases are expected to have been detected in the United States in 2007, with 15,280 deaths [3]. If diagnosed and treated early, when the cancer is confined to the ovary, the 5-year survival rate is more than 90%. Unfortunately, only 19% of cases are found at early stage [1]. Instead, most patients present with intraperitoneal (IP) disease, which forebodes poor prognosis [4,5]. After treatment, recurrence is common and most frequently occurs in the peritoneum.

Several small animal models have been developed to better understand ovarian cancer diagnosis and its progression and to evaluate new therapies. Among these, orthotopic models are preferred to more closely mimic human conditions. The most clinically relevant site for modeling orthotopic ovarian cancer is the peritoneal cavity because the peritoneal cavity is the principal site of disease in metastatic ovarian cancer; in addition, ovarian cancer commonly initially presents as IP metastasis [6,7]. Ovarian cancer is also one of the most common cancers to present as IP metastasis [8]. Localizing the primary tumor

Address all correspondence to: Vikas Kundra, MD, PhD., Diagnostic Radiology, The University of Texas MD Anderson Cancer Center, Box 0369, 1515 Holcombe Blvd, Houston, TX 77030. E-mail: vkundra@mdanderson.org

[1]This work was supported by Narional Institutes of Health grants P50 CA 83639 and P30 CA-016672.
Received 23 October 2008; Revised 16 February 2009; Accepted 17 February 2009

DOI 10.1593/tlo.08199

and assessing the extent of disease are critical during disease evaluation. However, IP tumors, unlike subcutaneous tumors, are not accessible for direct assessment; therefore, noninvasive imaging is needed.

A number of problems associated with tumor models may be addressed by imaging. For example, selecting animals with tumors before beginning experiments will reduce the number of animals needed for statistical significance and thus prove cost-effective given the expense of manufacturing therapeutics. In temporal experiments, it is common to sacrifice a subset of animals at each time point and perform histopathologic evaluation of the specimen. Tumors often have disparate growth rates, and sacrifice of the animal limits evaluation to a single time point instead of permitting individual lesions to be followed longitudinally [9]. Thus, serial imaging is needed to follow the natural history of disease and to assess therapeutic efficacy.

Clinically, computed tomography (CT) is most commonly used for staging ovarian cancer. However, unenhanced CT has the drawback of poor soft tissue contrast, which results in poor differentiation of tumor from the surrounding organs [10,11]. Commonly in patients, soft tissue resolution is improved by administering a bolus intravascular-extracellular intravenous contrast (IE-IV) agent, followed by rapid CT acquisition. This strategy is used in patients because scanning can be performed within seconds, allowing one to select when to image the contrast bolus. However, if the acquisition time is long, IV contrast equilibrates among tissues, resulting in a loss of tissue contrast. Traditionally, small animal CT is plagued by long acquisition times in the order of 15 to 20 minutes, thus alternative strategies are required.

An important advantage of CT is that it can be used to perform fusion imaging with functional imaging methods such as positron emission tomography (PET) and single photon emission computed tomography (SPECT). Hybrid machines using dual modalities with CT are available for small animals, which theoretically allow localization of functional signal [12]. However, this requires better visualization of individual organs and tumor in the abdomen and pelvis.

We used a negative contrast strategy to enhance normal tissue surrounding the tumor, instead of the more conventional approach of enhancing the tumor in particular. Normal tissues were enhanced by using various contrast agents and delivery routes, for example, oral contrast to enhance the stomach and the bowel, IP contrast to enhance the peritoneal space and outline the intra-abdominal structures, and intravenously delivered reticuloendothelial system–specific contrast (RES-IV) to enhance the liver and spleen. The purpose of our study was to assess whether a negative contrast strategy can be used to visualize and quantify IP tumor in a mouse model of ovarian cancer.

Materials and Methods

Cell Line and Culture

Ovarian cancer cells, Hey A8 (a kind gift from Dr. Gordon. B. Mills, Department of Systems Biology, The University of Texas MD Anderson Cancer Center, Houston, TX), were cultured in RPMI 1640 supplemented with 10% fetal bovine serum, 2 mM L-glutamine, 1× streptomycin-penicillin (Gibco BRL, Carlsbad, CA) at 37°C with 5% CO_2.

Animal Experiments

All animal experiments were approved by the Institutional Animal Care and Use committee. For IP injection, tumor cells were trypsinized, centrifuged at 1000 rpm × 7 minutes at 4°C, washed twice, and resuspended in serum free Hank's buffered salt solution (HBSS, Life Technologies, Rockville, MD) at a concentration of 2.5×10^6 cells/ml. Initially, IP tumors were established in nine nude mice. On the basis of a power calculation, 2.5 weeks later, the animals were randomly divided into groups of three animals each. At first, three mice were imaged by CT without any contrast agent (pre-mice). The animals were then given diatrizoate meglumine and diatrizoate sodium (Gastroview; Mallinckrodt, Inc, St. Louis, MO) at 45.8, 91.6, or 367 mg/ml (1:8 dilution, 1:4 dilution, or undiluted, respectively) *ad libitum* overnight. In the morning, these animals were administered 50, 150, or 300 μl of glyceryl 2-oleoyl 1, 3-bis [7-(3-amino-2, 4, 6-triiodophenyl)] alkanoate (Fenestra LC; Advanced Research Technologies, Inc, Montreal, Quebec, Canada) by tail vein injection (RES-IV, reticuloendothelial system–specific contrast). After 2 hours, 500 μl of oral diatrizoate meglumine and diatrizoate sodium was given by gavage at the same concentrations as overnight. Simultaneously, 400 μl of ioversol (Optiray 320; Mallinckrodt, Inc) was given IP in doses of 40, 80, or 320 mg/ml (1:8 dilution, 1:4 dilution, or undiluted, respectively). Thereafter, all animals were scanned by CT after 45 minutes to 1 hour. Data were used for Hounsfield unit (HU) measurement and radiologists' evaluation.

To test intravascular-extracellular IV contrast, based on a power calculation, another three animals with IP tumors were administered 300 μl of Optiray 320 (IE-IV) at 320 mg/ml by tail vein injection, and then imaged by CT immediately (capitalizing on the rapid 2-minute acquisition protocol; see Computed Tomography Protocol) as well as after a delay of 15 minutes (to evaluate the slower acquisition time of most small animal CT scanners). On the second day, oral Gastroview (367 mg/dl) was provided *ad libitum* overnight, followed by gavage with 500 μl at the same concentration in the morning. About 45 minutes to 1 hour later, they were administered 300 μl of IE-IV contrast at 320 mg/ml by tail vein injection, followed by immediate and delayed acquisition after 15 minutes. On the third day, the animals were given oral Gastroview (367 mg/dl) *ad libitum* overnight, followed by gavage with 500 μl at the same concentration in the morning. They were also administered 400 μl of IP Optiray 320 at 320 mg/ml. About 45 minutes to 1 hour later, they were administered 300 μl of IE-IV contrast at 320 mg/ml by tail vein injection, followed by immediate and delayed acquisition after 15 minutes. Data were used for HU measurement and radiologists' evaluation.

In another experiment, based on a power calculation, 15 animals were administered "standardized" doses of contrast: Gastroview (91.6 mg/ml) was provided *ad libitum* overnight. In the morning, the animals were administered 300 μl of RES-IV contrast by tail vein injection, followed 2 hours later by gavage with 500 μl of oral Gastroview at the same concentration as overnight and 400 μl of IP Optiray 320 at 320 mg/ml. About 45 minutes to 1 hour later, the animals were imaged by CT. From the CT images, tumor weight was calculated.

For all experiments, after imaging, animals were euthanized, digitally photographed, and the tumors excised and weighed.

Computed Tomography Protocol

The animals were imaged prone using an xSPECT-CT scanner (Gamma Medica, Flex XO xSPECT). High-resolution CT images were obtained at 75 kV and 310 μA current at a scanning time of 2 minutes per animal. The images have an isotropic voxel size of 170 μm at 250 milliseconds per frame for a total of 512 images per animal. AMIRA 3.1 was used to view and normalize the images, from which HUs were calculated using Image Segmentation editor. To control for potential partial voluming artifacts, the object of interest was seen in at least three contiguous slices, and the middle slice was used to assess HU.

Tumor Weight Measurement

Calculation of tumor weights was performed using ImageJ software, (http://rsb.info.nih.gov/ij, version 1.38) after converting the images into DICOM format. For assessing tumor volume, the periphery of the mass was manually traced on coronal images using a region of interest, and the area of the enclosed region was calculated. The area was then multiplied by the slice thickness to obtain the volume of the object of interest within a slice. To avoid overestimation of tumor size, one-half of the volume from the most dorsal and most ventral images containing tumor were used in the volume analysis. Assuming a tumor density of 1 g/ml, tumor volumes (mm^3) were converted to weight (g) for analysis. These were carried out by two individuals separately and at different times.

Radiologist Interpretation of Images

The images were arranged randomly, and blinded interpretation was done by two Board-certified radiologists individually and at different times, for tumor visualization, tumor margin delineation, and visualization of abdominal organs, including bladder, kidney, bowel, stomach, liver, spleen, and peritoneal cavity. The images were graded on a scale of 1 to 5 with 1 = not seen, 2 = poor, 3 = fair, 4 = good, and 5 = excellent. Images of all animals given serial dilutions of contrast, IE-IV contrast, and standardized doses of contrast were evaluated.

Statistics

Computed tomographic image HU measurements as well as organ/tumor HU ratios were log-transformed before analysis. A linear mixed model was used to assess the effect of contrast agents on HU measurements and HU ratios. The Wilcoxon rank sum test was used to compare image quality ratings across contrast groups. The Spearman's correlation test was used to correlate CT-derived *in vivo* tumor weight with *ex vivo* tumor weight. Bland-Altman analysis was performed. All tests were two-sided, and P values of 0.05 or lower were considered statistically significant. Statistical analysis was carried out using SAS version 9 (SAS Institute, Cary, NC) and S-Plus 7 (Insightful, Inc, Seattle, WA).

Results

Representative Images

Representative coronal *in vivo* CT images of mice bearing IP Hey A8 tumor given different doses of oral contrast, IP contrast, and RES-IV contrast are shown in Figure 1*A*. In the pre-mice (without any contrast agent), it was difficult to delineate the tumor because of poor soft tissue contrast. In addition, there was poor differentiation among almost all organs such as liver, stomach, spleen, bowel, and bladder. In general, as the concentration of oral Gastroview, IP Optiray 320, and RES-IV contrasts increased, the tumor was better visualized, and the margins were better delineated from the surrounding organs.

Figure 1*B* shows immediate and delayed acquisition *in vivo* CT images of mice bearing IP Hey A8 tumor after administration of IE-IV, oral, and IP contrasts. The tumor adjacent to the bladder was well visualized, and its margins were well delineated in both the immediate and delayed acquisition images. However, the tumor and its margins adjacent to the liver, spleen, and stomach were not as well seen on either the immediate or the delayed imaging.

Organ/Tumor Enhancement

The dose dependency of contrast enhancement in the different organs was assessed by HU measurements (Figure 2*A*). With increasing doses of oral Gastroview, the HU of stomach and bowel increased significantly. The HU of bowel plateaued at the lowest dose of oral Gastroview (45.8 mg/ml), whereas the HU of stomach further increased with increasing doses of oral Gastroview. Administration of RES-IV contrast resulted in a significant increase in the HU of the liver and spleen. With increasing doses of IP Optiray 320, peritoneal HU increased; this was also found in the renal cortex and renal pelvis. The HU of the bladder plateaued at the lowest dose of IP Optiray 320, 40 mg/ml, consistent with concentrated material in urine. In contrast, the HU of tumor increased only slightly. Mineralized bone was used as a control because none of the contrast strategies were targeted to mineralized bone. As expected, cortical bone did not show any significant difference in enhancement regardless of contrast administration. Thus, upon administering increasing doses of contrasts, there was generally an increase in enhancement of all abdominal organs. In comparison, tumor HU increase was minimal.

Upon administering IE-IV contrast, along with oral Gastroview and IP Optiray 320 in successive combinations (Figure 2*B*), similar results were obtained. The HU of stomach and bowel increased significantly upon administering oral Gastroview along with IE-IV contrast. The HU of the peritoneum increased significantly upon administering IE-IV contrast; but HU markedly increased upon addition of IP Optiray 320. Further, the 15-minute delayed imaging resulted in greater peritoneal HU compared with immediate imaging. The HU of liver, renal cortex, and renal pelvis increased significantly upon administering IE-IV contrast alone and with coadministration of IP Optiray 320. In contrast, the HU of tumor increased slightly. The HU of control cortical bone did not show any significant difference in enhancement, as expected.

Tumor Enhancement Compared with Organ Enhancement

Tumor HU in relation to that of surrounding organs at different doses of contrast is compared in Figure 3, *A* and *B*. In the pre-mice, without any contrast administered, the HU of the tumor was not significantly different from surrounding organs, except bladder, where there is a minimal difference, and an expected large difference compared with bone. As seen in Figure 3*A*, upon administering oral Gastroview, IP Optiray 320, and RES-IV contrasts in increasing doses, the HU of abdominal and pelvic organs increased significantly relative to that of tumor, and this, in general, was magnified by increasing contrast dose. The high HU values in the bladder are expected owing to the IP contrast uptake by the peritoneal lining into the vascular system and this intravenous contrast being concentrated by the kidneys and excreted into the urine. In comparison, the HU of bone remained relatively stable. Thus, the HU of abdominal organs showed a statistically significant increase relative to the tumor, and this was dependent on the doses of contrasts.

A similar trend was seen on administering IE-IV contrast successively in combination with oral Gastroview and IP Optiray 320 (Figure 3*B*). Addition of contrasts significantly increased the HU of surrounding abdominal and pelvic organs compared with tumor.

Ratio of Organ to Tumor Enhancement

To further assess tumor to organ distinction, the ratios of HU of adjacent organs to tumor adjacent to liver, spleen, and stomach were evaluated. Representative organs targeted by the different contrast

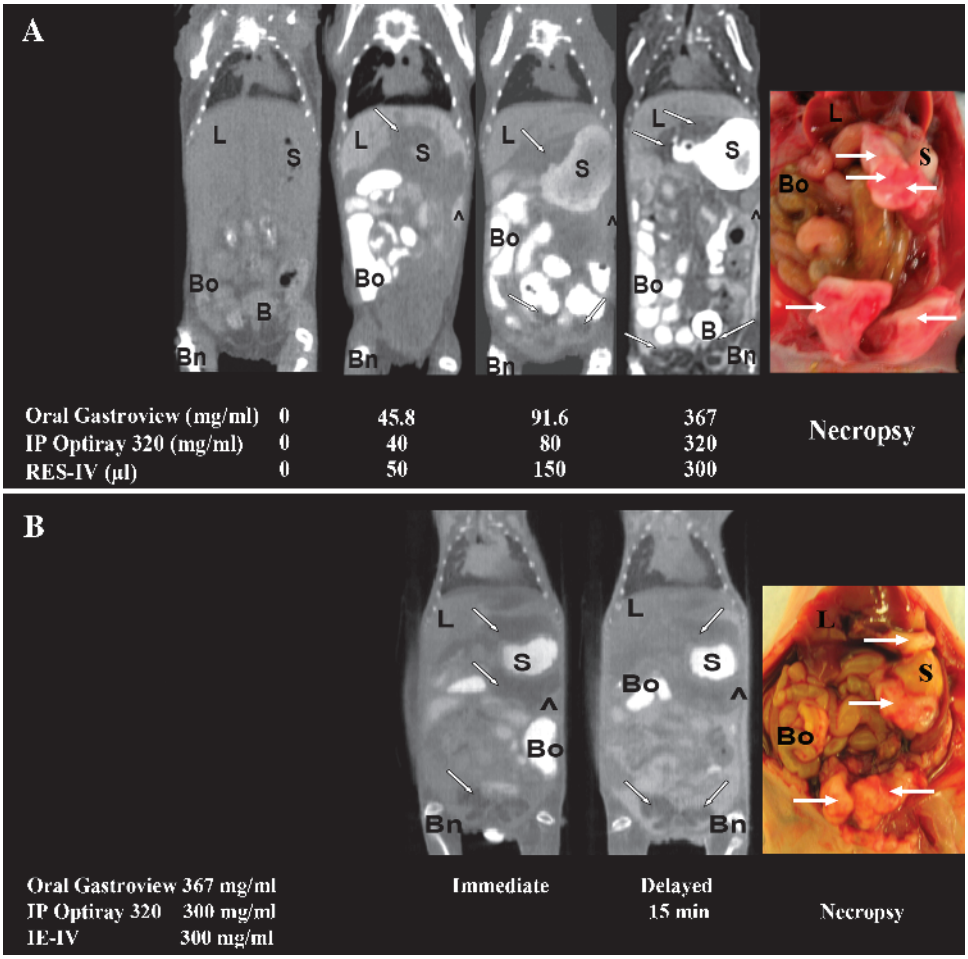

Figure 1. (A) Representative white light and *in vivo* CT images of IP Hey A8 tumors before and after administration of different doses of oral, IP, and RES-IV contrasts. (B) Representative immediate and delayed (15 minutes) *in vivo* CT images and white light images of IP Hey A8 tumors in mice administered oral, IP, and IE-IV contrasts. In the pre-mice, without any contrast, tumor and other organs are not well visualized. Upon administering contrasts, tumor and organs are better visualized. Tumor appears as areas of low attenuation compared with adjacent structures. ^ indicates peritoneum; B, bladder; Bn, bone; Bo, bowel; L, liver; S, stomach.

agents are plotted in Figure 4*A*. In the pre-mice, the ratios of bowel, liver, spleen, and peritoneum to tumor adjacent to liver, spleen, and stomach were close to 1, confirming poor tissue organ distinction. As the doses of the contrast agents increased, the ratios in general increased as well (i.e., adjacent organs showed greater enhancement than tumor) suggesting a dose-dependent response. The ratio of bowel to tumor became statistically significantly different at 45.8 mg/ml of oral Gastroview, consistent with the difference in HU of bowel at the same concentration in Figure 2*A*. The ratio of peritoneum to tumor increased to the highest doses used. The ratio of spleen to tumor showed a similar trend. The ratio of liver to tumor became statistically significantly different at the lowest dose of RES-IV contrast, again consistent with the increase in liver HU seen in Figure 2*A*. In keeping with the mild increase in tumor HU, the ratio of bone to tumor decreased slightly with increasing doses of contrasts. Thus, the ratios of enhancement of adjacent structures like liver, spleen, bowel, and peritoneum to tumor adjacent to the liver, spleen, and stomach statistically significantly increases and can plateau with increasing doses of contrasts.

Figure 4*B* compares HU ratios of selected organs to tumor adjacent to the liver, spleen, and stomach in mice administered oral, IP, and RES-IV contrasts *versus* HU ratios after immediate or delayed imaging of mice administered oral, IP, and IE-IV contrasts. The ratio of HU of spleen to tumor was significantly higher with the RES-IV regimen compared with both immediate and delayed imaging with the IE-IV regimen. The ratio of HU of liver to tumor also showed a similar trend. The ratio of HU of bowel to tumor and peritoneum to tumor increased significantly compared with pre-mice upon administering contrast, but the ratio was not statistically different among the contrast regimens.

Qualitative Assessment

Qualitative assessment of the visualization of the IP tumor, its margins, and of surrounding abdominal structures was performed by two Board-certified radiologists. The tumor and its margins were not seen in the pre-mice but were excellently seen in the mice given the highest doses of contrasts or the standardized dose of the RES-IV contrast regimen (Figure 5*A*). Visualization of all organs improved significantly with contrasts compared with without contrast (Figure 5*B*).

Stomach and bowel were well to excellently visualized at a dose of 91.6 mg/ml of oral Gastroview. Adding oral contrast to RES-IV or IE-IV contrasts permitted fair to good visualization of stomach and bowel. Peritoneum, bladder, and kidney visualization was fair to excellent at 80 mg/ml of IP Optiray 320. The visualization of liver and spleen was fair to good even at the lowest dose of RES-IV contrast.

Tumor and the abdominal organs were well to excellently visualized in the mice administered standardized doses of contrasts. The visualization of bladder and kidney was fair to excellent even in mice administered IE-IV contrast alone. Visualization of the peritoneum improved by adding IP Optiray 320 to IE-IV contrast.

As seen in Figure 5*C*, visualization and margin delineation of tumor adjacent to the liver, spleen, and stomach were significantly better upon administering RES-IV contrast with oral Gastroview and IP Optiray 320 at the standardized dose compared with immediate or delayed imaging using IE-IV contrast with oral Gastroview and IP Optiray 320. No difference was seen for tumor adjacent to the bladder.

Intraperitoneal Tumor Quantification

Next, we evaluated the ability of the negative contrast CT imaging method to quantify tumor burden. For this part of the study, standardized doses of 91.6 mg/ml of oral Gastroview, 320 mg/ml of IP Optiray 320, and 300 μl of RES-IV contrasts were administered. Tumor weights derived from CT images correlated strongly with weights of excised tumors ($r = 0.96$, $P < .0001$, coefficient of the

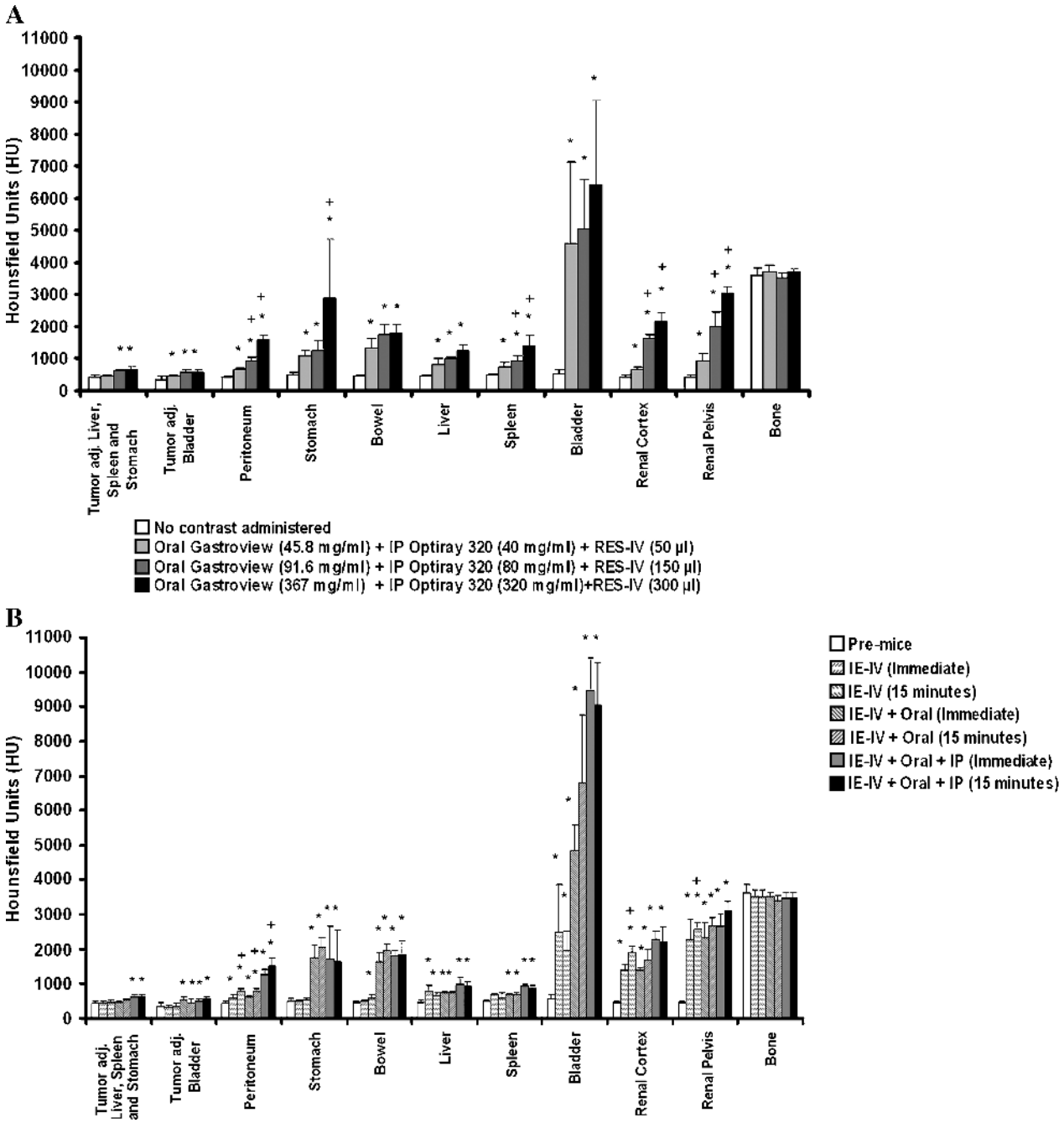

Figure 2. (A) Quantification of HU in tumors and individual organs after administration of different doses of RES-IV, oral, and IP contrasts. (B) Quantification of HU in tumors and individual organs after administration of IE-IV, oral, and/or IP contrast combinations. In general, the HU of organs increased with increasing amounts of contrasts; in comparison, the HU of tumor increased only minimally. *$P < .05$ of dose compared with pre-mice with no contrast administered, within the same organ or tumor. (A) $^{+}P < .05$ of dose compared with previous dose within the same organ or tumor. (B) $^{+}P < .05$ of dose comparing immediate to delayed imaging within the same organ or tumor.

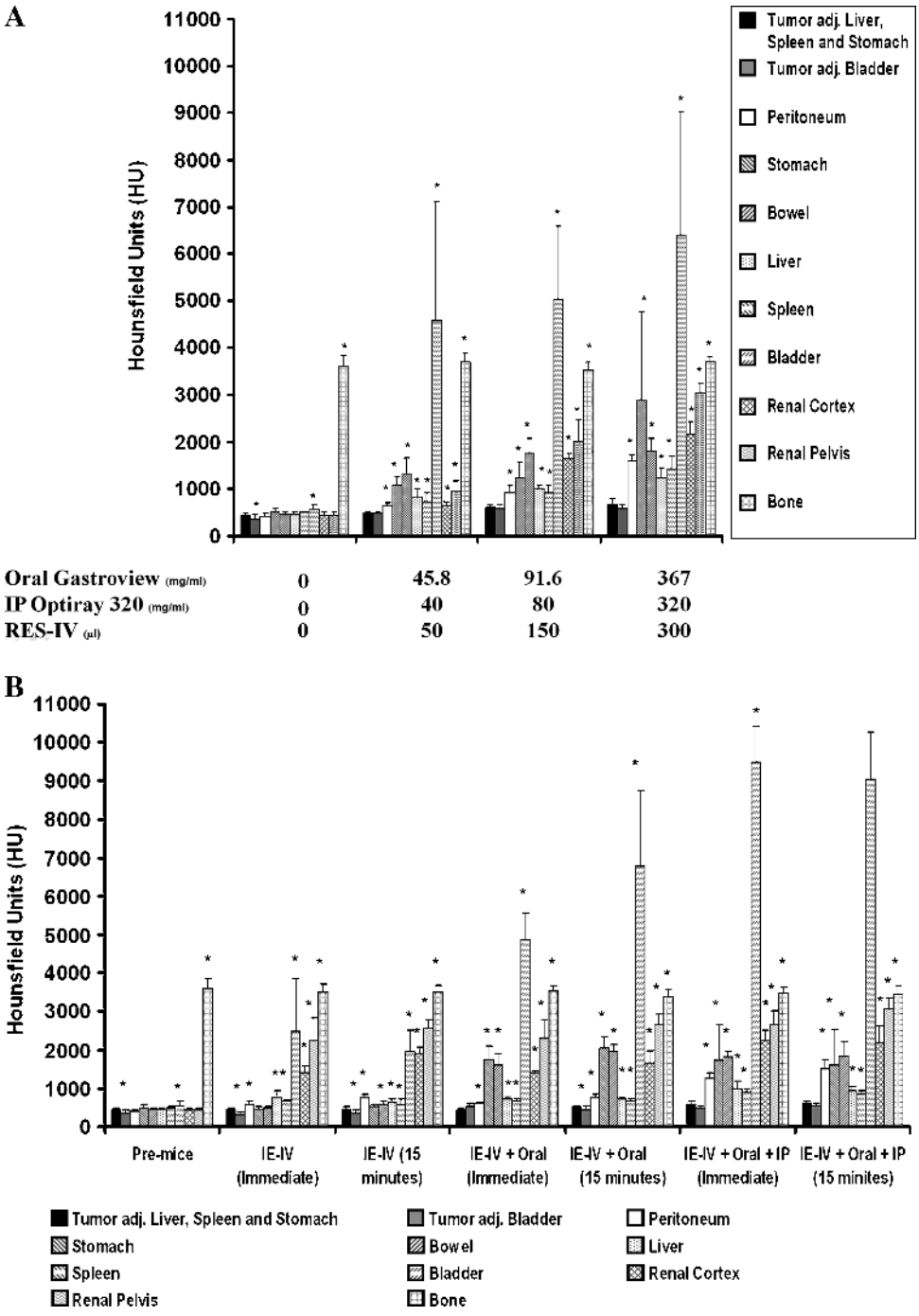

Figure 3. (A) Comparison of tumor HU to that of surrounding organs before and after administration of different doses of oral, IP, and RES-IV contrasts. (B) Comparison of tumor HU to that of surrounding organs before and after administration of oral, IP, and IE-IV contrasts after the immediate or a 15-minute delayed imaging. In the pre-mice, tumor HU is primarily similar to HU of surrounding organs. Generally, with increasing amounts of contrasts, tumor HU becomes significantly lower than that of surrounding organs. *$P < .05$ compared with tumor adjacent to the liver, spleen, and stomach.

x variable = 1.18, *n* = 15; Figure 6*A*). Similar results were obtained by a second independent reader ($r = 0.95$, $P < .0001$, coefficient of the *x* variable = 1.06, *n* = 15; data not shown). These findings suggest that using the negative contrast strategy, IP tumors can be quantified.

The Bland-Altman analysis was performed of the data in Figure 6*A* to compare *ex vivo* tumor weight with *in vivo* CT-derived tumor weight. As shown in Figure 6*B*, the *in vivo* CT-derived tumor weight was on average 0.09 g (±2SD: −0.04 to 0.21) smaller than the *ex vivo* tumor weight. The correlation is quite high, and the coefficient of the *x* variable suggests that a correction factor of 1.18 may be used when converting *in vivo* CT-derived tumor weight to *ex vivo* tumor weight.

Discussion

Computed tomography, in conjunction with the negative contrast strategy, can visualize and quantify IP tumor. Ovarian cancer most

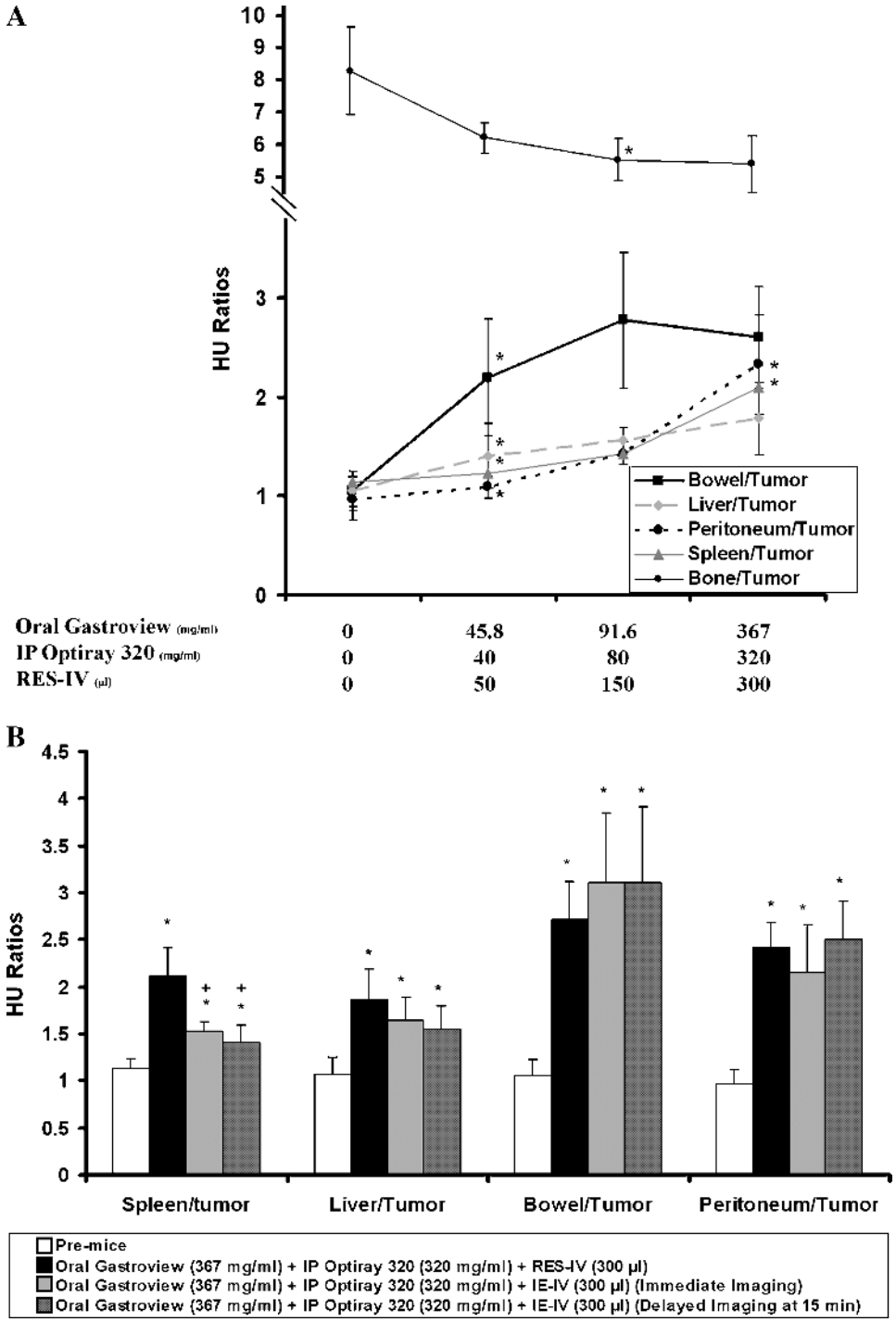

Figure 4. (A) Ratio of surrounding organ HU to HU of tumor adjacent to liver, spleen, and stomach with different doses of contrast. In the pre-mice, ratios are close to 1 but, in general, increase with increasing doses of contrast. Bone to tumor HU ratio changes minimally. $^{*}P <$ .05 of ratio compared with the ratio at the previous dose within the same organ to tumor. (B) Comparison of ratios of HU of spleen, liver, bowel, and peritoneum to tumor adjacent to the liver, spleen, and stomach in mice administered oral, IP, and RES-IV contrasts at the highest dose, with immediate and delayed imaging of mice administered oral, IP, and IE-IV contrasts. Ratio of HU of spleen to tumor is significantly higher with the RES-IV regimen compared with both immediate and delayed imaging with the IE-IV regimen. $^{*}P < .05$ comparing ratio to pre-mice. $^{+}P < .05$ comparing ratio for RES-IV regimen to IE-IV regimen.

Figure 5. (A and B) Visualization of tumor and organs improves significantly with contrasts. $^{*}P < .05$ of dose compared with pre-mice without any contrast. $^{+}P < .05$ comparing to previous dose within the same organ or tumor. (C) Visualization of tumor and its margins in mice administered oral, IP, and RES-IV contrasts undiluted or at the standardized dose compared with immediate and delayed imaging of mice administered oral, IP, and IE-IV contrasts. Visualization and margin delineation of tumor adjacent to the liver, spleen, and stomach are significantly better in mice administered the RES-IV regimen. For tumor near the bladder, no difference was seen. $^{*}P < .05$ compared with standardized dose.

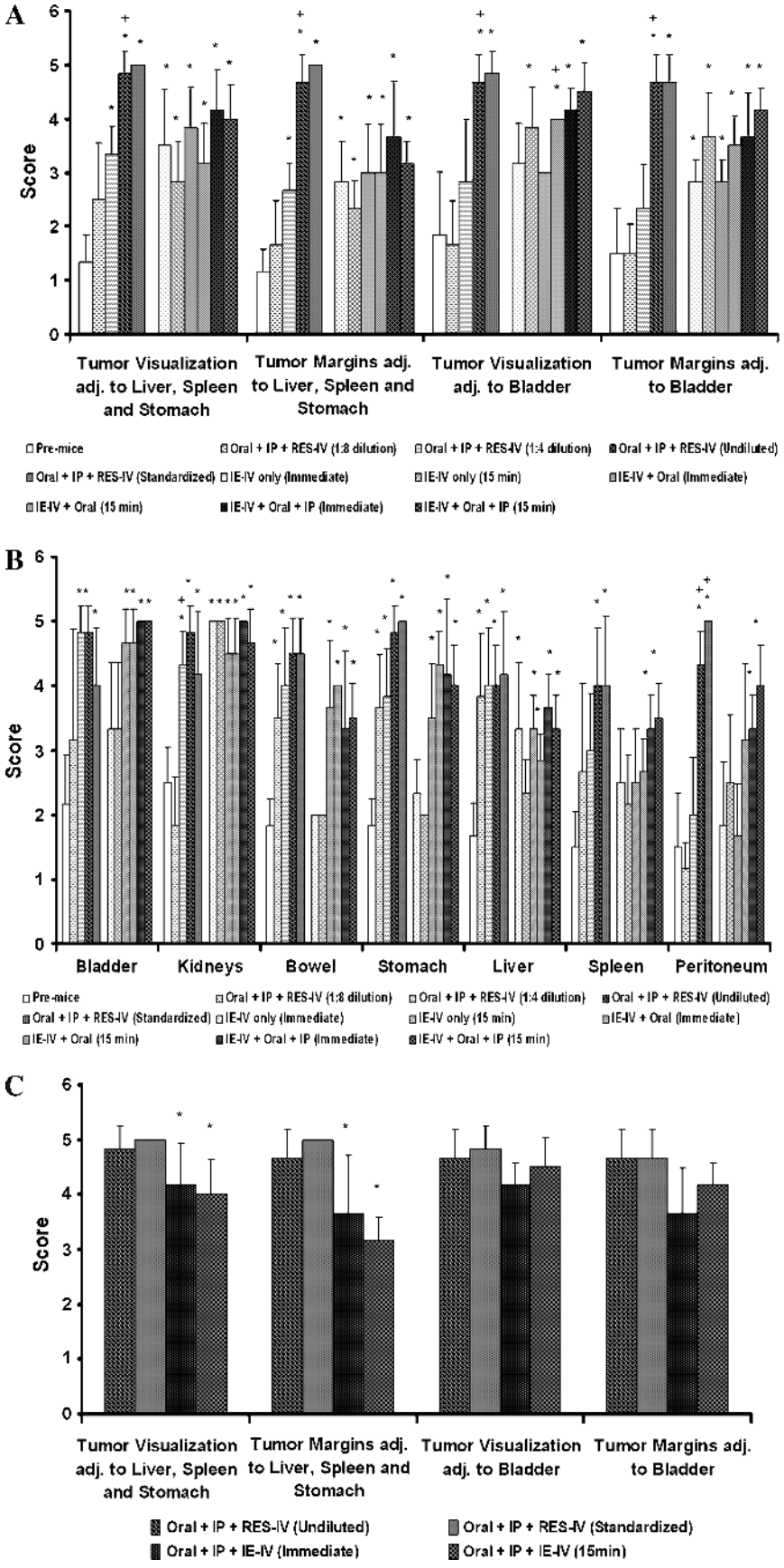
A
Score
Tumor Visualization adj. to Liver, Spleen and Stomach
Tumor Margins adj. to Liver, Spleen and Stomach
Tumor Visualization adj. to Bladder
Tumor Margins adj. to Bladder
Pre-mice
Oral + IP + RES-IV (1:8 dilution)
Oral + IP + RES-IV (1:4 dilution)
Oral + IP + RES-IV (Undiluted)
Oral + IP + RES-IV (Standardized)
IE-IV only (Immediate)
IE-IV only (15 min)
IE-IV + Oral (Immediate)
IE-IV + Oral (15 min)
IE-IV + Oral + IP (Immediate)
IE-IV + Oral + IP (15 min)
B
Score
Bladder
Kidneys
Bowel
Stomach
Liver
Spleen
Peritoneum
Pre-mice
Oral + IP + RES-IV (1:8 dilution)
Oral + IP + RES-IV (1:4 dilution)
Oral + IP + RES-IV (Undiluted)
Oral + IP + RES-IV (Standardized)
IE-IV only (Immediate)
IE-IV only (15 min)
IE-IV + Oral (Immediate)
IE-IV + Oral (15 min)
IE-IV + Oral + IP (Immediate)
IE-IV + Oral + IP (15 min)
C
Score
Tumor Visualization adj. to Liver, Spleen and Stomach
Tumor Margins adj. to Liver, Spleen and Stomach
Tumor Visualization adj. to Bladder
Tumor Margins adj. to Bladder
Oral + IP + RES-IV (Undiluted)
Oral + IP + RES-IV (Standardized)
Oral + IP + IE-IV (Immediate)
Oral + IP + IE-IV (15min)

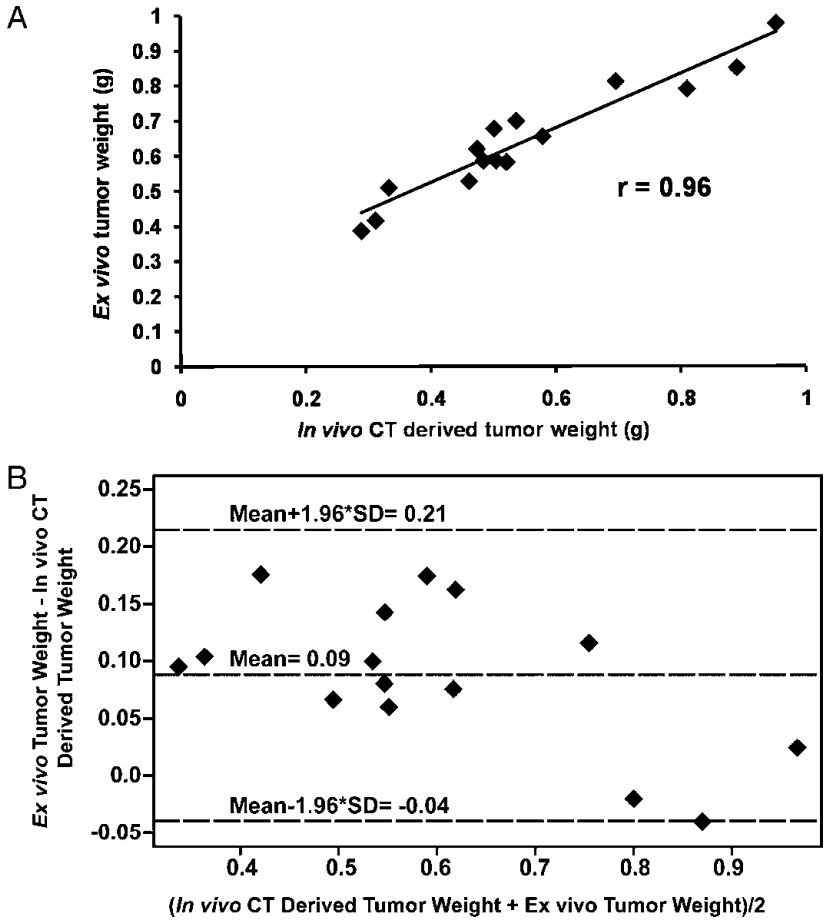

Figure 6. (A) Correlation between *in vivo* CT-derived tumor weights and *ex vivo* tumor weights ($r = 0.96$, $P < .0001$, coefficient of the x variable = 1.18, $n = 15$). (B) Bland-Altman Analysis comparing *in vivo* CT-derived tumor weights and *ex vivo* tumor weights.

commonly presents as IP tumors in patients [4,5]. Intraperitoneal tumors are not accessible for direct visualization and measurement by traditional methods, such as calipers, and therefore need imaging for evaluation of tumor development, progression, and response to various therapeutic modalities [13,14].

Unenhanced CT has poor soft tissue contrast resolution. In patients, IE-IV is routinely used to enhance the tumor with rapid CT acquisition within 1 to 2 minutes of injection. Coakley et al. [8] reported a sensitivity of 85% to 93% in detecting peritoneal metastases in patients with ovarian cancer using high-speed spiral CT scanners after giving oral and IE-IV contrast. Administration of IP contrast further increases sensitivity in detecting peritoneal metastasis from gynecologic malignancies in patients [15,16].

Owing to the slow speed of most traditional small animal scanners, which leads to equilibration of IE-IV contrast, such an IV contrast strategy is not applicable in a majority of animal models. This is supported by the findings of Weber et al. [17] in their study on imaging murine liver tumor using micro-CT. They concluded that imaging intra-abdominal tumors was difficult in animal models because of a lack of soft tissue contrast between organs. The long acquisition time (approx. 20 minutes) associated with most micro-CT scanners precluded the use of conventional water-soluble IE-IV agents.

We used a negative contrast strategy to visualize IP tumors in animal models, which enhances the organs surrounding the tumor rather than the tumor itself. Because we used a fast scanner, with an acquisition time of 2 minutes per animal, we also tested an IE-IV contrast imaging strategy, followed by immediate and delayed CT acquisition after 15 minutes.

Administration of IP contrast opacifies the peritoneal cavity, which can provide visualization of boundaries between organs [18], and we hypothesized better distinction of the tumor. However, the organs and tumor may still oppose each other, limiting distinction. Martiniova et al. [14] reported that unenhanced CT showed a uniform density of soft tissue structures in animal models and suggested that administration of Fenestra LC (RES-IV) through the tail vein can enhance normal liver compared with a tumor within the liver. We reasoned that RES-IV can be used to visualize the boundaries of the liver and spleen. Bowel, including stomach, can also mimic tumor. To fill the bowel, oral contrast was provided *ad libitum* overnight. Because oral contrast may quickly pass from the stomach to the small bowel, we also gave oral contrast by gavage, 45 minutes to 1 hour before the scan.

Tumors were established by IP injection of human ovarian cancer cell line Hey A8. In the first set of experiments, before imaging, mice were administered oral contrast (Gastroview), IP contrast (Optiray 320), and IV reticuloendothelial system–specific contrast agent (Fenestra LC, RES-IV). The oral contrast fills the stomach and bowel, allowing its visualization. The oral contrast does not escape the bowel. Intraperitoneal contrast fills the IP cavity and converts the potential space of the IP cavity into a real space filled with contrast. This outlines the IP organs and tumor. It enters slowly, but to a small degree into the

vascular system through the peritoneal lining, which allows visualization of the kidneys because the kidneys concentrate the now intravenous contrast during the process of urine excretion. We noted that the kidney contrast increased with IP Optiray 320, with or without concurrent RES-IV contrast (data not shown). RES-IV, which is a lipid-based formulation, enhances RES organs such as the liver and the spleen. Fat, which is easily identifiable by its low attenuation and known anatomic distribution, was not enhanced. These three contrast strategies are specifically designed to outline or enhance normal organs that abut the ovarian tumor. They are also specifically designed not to enhance the tumor in the peritoneal cavity because the tumor does not fit the categories above. The unenhanced tumor on imaging was confirmed at resection, and the image-derived tumor weight correlated highly with excised tumor weight. Bone was used as a control because it was not targeted by the contrast strategy, and its HU remained stable regardless of the contrast regimens.

In pre-mice, without any contrast, there was no significant difference in the HU of tumor compared with that of surrounding organs. With increasing doses of contrast, a significant increase occurred in the HU of abdominal organs surrounding the tumor, allowing better visualization and delineation of tumor. A slight increase in enhancement of the tumor was seen, which we believe is due to the IP Optiray 320 entering the tumor through the vasculature. This was minor and did not limit tumor conspicuity.

For the IE-IV contrast imaging strategy, mice with IP tumors were administered IV Optiray 320 (IE-IV), oral Gastroview, and IP Optiray 320 in successive combinations. The addition of oral contrast significantly increased the HU of the stomach and bowel. The HU of the peritoneum increased upon administering IE-IV contrast, and this was greater on delayed imaging because of a leak of contrast into the peritoneal cavity. Adding IP contrast increased peritoneal HU further. The HU of liver, spleen, renal cortex, and renal pelvis increased significantly with the administration of IE-IV contrast alone. The HU of the tumor on administering IE-IV contrast enhanced only slightly implying that the tumors are not very vascular. Hypovascular tumors are appreciated as low attenuation in the liver after IV contrast in the portovenous phase because the liver takes up more contrast compared with the tumor. For vascular tumors, IE-IV contrast may worsen visualization by causing equalization of enhancement between tumor and normal viscera.

The ratios of liver, spleen, bowel, and peritoneum to tumor, which were close to 1 in the pre-mice, increased significantly upon giving the different contrast agents, thus improving soft tissue discrimination. This corresponded with the findings of two Board-certified radiologists in evaluating tumor visualization, tumor margins, and the visualization of abdominal organs surrounding the tumor. In general, increasing concentrations of the contrast improved tumor visualization and tumor margin delineation.

For visualizing individual organs, good to excellent visualization was achieved for each organ. In general, visualization improved with increasing dose, but for some, a plateau was reached. In the case of liver and spleen, visualization was fair to good even at the lowest dose. This highlights the importance of qualitative assessment of visualization and suggests potential cost savings. Further, high contrast concentrations have the potential to cause artifacts, such as beam hardening. The kidneys could be visualized even in the absence of contrast because of the surrounding perinephric fat; however, the IP contrast improved their visualization. The visualization of the tumor adjacent to the liver, spleen, and stomach and the delineation of its margins were excellent in mice administered oral, IP, and RES-IV contrasts at the standardized dose. This was significantly better than using oral, IP, and IE-IV contrasts. This improvement is due to better distinction of tumor from surrounding viscera, liver, and spleen, which are enhanced by the RES-specific agent. This is further corroborated by the ratios of HU of spleen to tumor being statistically significantly higher in mice administered RES-IV contrast compared with mice administered IE-IV contrast. The ratios of HU of liver to tumor showed a similar trend. For visualization and margin delineation of tumor adjacent to the bladder, imaging with IE-IV or RES-IV contrast agents plus oral and IP contrast was equivalent owing to the absence of any opposing adjacent organs with similar enhancement in the pelvis.

We also evaluated the ability of the negative contrast CT strategy to quantify IP tumor burden. Tumor weights measured *ex vivo* were used as the criterion standard. We previously showed that magnetic resonance (MR) imaging of IP tumors correlates strongly with *ex vivo* tumor weights ($r = 0.97$, $P < .001$) [19]. In the present study, we obtained a similar significant correlation between the tumor weights obtained by *in vivo* CT imaging and the tumor weights *ex vivo*. Bland-Altman analysis, performed to compare *ex vivo* tumor weight with *in vivo* CT-derived tumor weight, showed that the *in vivo* CT-derived tumor weight was on average 0.09 g (±2SD: −0.04 to 0.21) smaller than the *ex vivo* tumor weight. The correlation is quite high, and the coefficient of the x variable suggests that a slight correction factor may be used when converting *in vivo* CT-derived tumor weight to *ex vivo* tumor weight. The high degree of correlation ($r = 0.96$, $P < .001$) enables longitudinal imaging for following the natural history of disease and the efficacy of therapeutic intervention. Although we used ovarian cancer as a model, we expect that this technique can be applied to other IP tumor models such as for colon cancer, liver cancer, pancreatic cancer, and breast cancer.

Owing to its noninvasive nature, CT can be performed in living mice serially. In terms of radiation dose, the animals were exposed to approximately 0.2 cGy per CT scanning session using the xSPECT-CT scanner (personal communication from the manufacturer, Gamma Medica). The sensitivity of different strains of mice to radiation varies. Budach et al. [20] reported that the LD_{50} of radiation for severe combined immune deficiency mice is 3 Gy compared with 7.8 Gy for nonimmunosuppressed mice. Sublethal whole body irradiation results in damage to the bone marrow and hematopoietic stem cells. In the spleen, this results in the production of colony-forming units (CFU-S), which have been used as a measure of radiation sensitivity. In normal mice, CFU-S appear at approximately 6 Gy, whereas in severe combined immune deficiency mice, CFU-S appear at 3 Gy [21]. The low radiation dose used in this study implies that multiple sessions of CT imaging can be performed without significant injury to the animal.

An important advantage of CT is that it can be used to perform fusion imaging with functional imaging methods such as PET and SPECT. Fusion imaging allows localization of functional signal. Hybrid machines using dual modalities with CT are now available for small animals. However, many of these CTs are plagued by long acquisition times and have limited visualization of intra-abdominal organs. In an earlier study demonstrating the antitumor effects of a vascular disrupting agent in IP ovarian cancer models, we have shown that combination imaging using MR and PET can be used to demonstrate effect of therapy not only anatomically but also metabolically; however, integrated MR/PET or MR/SPECT scanners are not yet generally available for animal models, necessitating individual imaging by the different imaging modalities [19]. This limits coregistration of

images, and it is practically difficult to obtain near-simultaneous imaging. In terms of PET-CT, Tatsumi et al. [22] reported that combined PET/CT, using a clinical imaging machine, can be used for sequential noninvasive imaging of liver tumors in rabbits. In another animal study, we have demonstrated that combining functional and anatomic imaging by small animal machines can also be used for noninvasive quantification of gene expression in tumors, such as fibrosarcomas; for anatomic imaging, MR was used to obtain high soft tissue contrast [23]. Thus, combined anatomic and functional imaging using the negative contrast strategy should prove useful for a variety of applications.

The value of combined anatomic and functional imaging has also been demonstrated in the clinic. In a prospective clinical study on the diagnostic value of ^{18}F-FDG-PET/CT for primary ovarian cancer in patients, Risum et al. [24] reported a sensitivity of 100% in detecting a malignant pelvic tumor and a specificity of 92.5% compared with pathologic examination. Hauth et al. [25], evaluating ^{18}F-FDG-PET/CT for detecting ovarian cancer in patients, reported that the combination of PET with CT, which added functional information to morphology, enabled a better differentiation of tumor. Further, combined ^{18}F-FDG-PET/CT imaging has been reported to be more sensitive for detecting recurrent ovarian cancer in patients than either modality alone [26–29]. Our triple-contrast strategy should enable localization of multiple different functional signals that may originate in the abdomen or pelvis.

Computed tomography using the negative contrast enhancement strategy can be used for visualization and quantification of IP tumors. The negative enhancement CT technique enables longitudinal assessment for studying the biology of the disease and response to therapy. These techniques should enable localization of IP cancers using both fast and slow CT scanners.

References

[1] National Ovarian Cancer Coalition Inc. What everyone should know about ovarian cancer. Available at: http://www.ovarian.org/images/23bcOeveryone shouldknow.pdf.

[2] Landis SH, Murray T, Bolden S, and Wingo PA (1998). Cancer statistics. *CA Cancer J Clin* **48**, 6–29.

[3] American Cancer Society (2007). Cancer Facts and Figures. Atlanta: American Cancer Society.

[4] Mesiano S, Ferrara N, and Jaffe RB (1998). Role of vascular endothelial growth factor in ovarian cancer: inhibition of ascites formation by immunoneutralization. *Am J Pathol* **153**, 1249–1256.

[5] Forstner R, Hricak H, Occhipinti KA, Powell CB, Frankel SD, and Stern JL (1995). Ovarian cancer: staging with CT and MR imaging. *Radiology* **197**, 619–626.

[6] Cannistra SA (2004). Cancer of the ovary. *N Engl J Med* **351**, 2519–2529.

[7] Thigpen T (2004). The if and when of surgical debulking for ovarian carcinoma. *N Engl J Med* **351**, 2544–2546.

[8] Coakley FV, Choi PH, Gougoutas CA, Pothuri B, Venkatraman E, Chi D, Bergman A, and Hricak H (2002). Peritoneal metastases: detection with spiral CT in patients with ovarian cancer. *Radiology* **223**, 495–499.

[9] Kundra V, Ng CS, Ma J, Bankson JA, Price RE, Cody DD, Do KA, Han L, and Navone NM (2007). *In vivo* imaging of prostate cancer involving bone in a mouse model. *Prostate* **67**, 50–60.

[10] Frasci G, Contino A, Iaffaioli RV, Mastrantonio P, Conforti S, and Persico G (1994). Computerized tomography of the abdomen and pelvis with peritoneal administration of soluble contrast (IPC-CT) in detection of residual disease for patients with ovarian cancer. *Gynecol Oncol* **52**, 154–160.

[11] Giunta S, Tipaldi L, Diotellevi F, Squillaci E, Cecconi L, Nardis PF, and Squillaci S (1990). CT demonstration of peritoneal metastases after intraperitoneal injection of contrast media. *Clin Imaging* **14**, 31–34.

[12] Meikle SR, Kench P, Kassiou M, and Banati RB (2005). Small animal SPECT and its place in the matrix of molecular imaging technologies. *Phys Med Biol* **50**, R45–R61.

[13] Zavaleta CL, Phillips WT, Bradley YC, McManus LM, Jerabek PA, and Goins BA (2007). Characterization of an intraperitoneal ovarian cancer xenograft model in nude rats using noninvasive microPET imaging. *Int J Gynecol Cancer* **17**, 407–417.

[14] Martiniova L, Ohta S, Guion P, Schimel D, Lai EW, Klaunberg B, Jagoda E, and Pacak K (2006). Anatomical and functional imaging of tumors in animal models: focus on pheochromocytoma. *Ann N Y Acad Sci* **1073**, 392–404.

[15] Halvorsen RA Jr, Panushka C, Oakley GJ, Letourneau JG, and Adcock LL (1991). Intraperitoneal contrast material improves the CT detection of peritoneal metastases. *AJR Am J Roentgenol* **157**, 37–40.

[16] Gryspeerdt S, Clabout L, Van Hoe L, Berteloot P, and Vergote IB (1998). Intraperitoneal contrast material combined with CT for detection of peritoneal metastases of ovarian cancer. *Eur J Gynaecol Oncol* **19**, 434–437.

[17] Weber SM, Peterson KA, Durkee B, Qi C, Longino M, Warner T, Lee F, and Weichert J (2004). Imaging of murine liver tumor using microCT with a hepatocyte-selective contrast agent: accuracy is dependent on adequate contrast enhancement. *J Surg Res* **119**, 41–45.

[18] Paulus MJ, Gleason SS, Kennel SJ, Hunsicker PR, and Johnson DK (2000). High resolution X-ray computed tomography: an emerging tool for small animal cancer research. *Neoplasia* **2**, 62–70.

[19] Kim TJ, Ravoori M, Landen CN, Kamat AA, Han LY, Lu C, Lin YG, Merritt WM, Jennings N, Spannuth WA, et al. (2007). Antitumor and antivascular effects of AVE8062 in ovarian carcinoma. *Cancer Res* **67**, 9337–9345.

[20] Budach W, Hartford A, Gioioso D, Freeman J, Taghian A, and Suit HD (1992). Tumors arising in SCID mice share enhanced radiation sensitivity of SCID normal tissues. *Cancer Res* **52**, 6292–6296.

[21] Fulop GM and Phillips RA (1990). The scid mutation in mice causes a general defect in DNA repair. *Nature* **347**, 479–482.

[22] Tatsumi M, Nakamoto Y, Traughber B, Marshall LT, Geschwind JF, and Wahl RL (2003). Initial experience in small animal tumor imaging with a clinical positron emission tomography/computed tomography scanner using 2-[F-18] fluoro-2-deoxy-D-glucose. *Cancer Res* **63**, 6252–6257.

[23] Yang D, Han L, and Kundra V (2005). Exogenous gene expression in tumors: noninvasive quantification with functional and anatomic imaging in a mouse model. *Radiology* **235**, 950–958.

[24] Risum S, Hogdall C, Loft A, Berthelsen AK, Hogdall E, Nedergaard L, Lundvall L, and Engelholm SA (2007). The diagnostic value of PET/CT for primary ovarian cancer—a prospective study. *Gynecol Oncol* **105**, 145–149.

[25] Hauth EA, Antoch G, Stattaus J, Kuehl H, Veit P, Bockisch A, Kimmig R, and Forsting M (2005). Evaluation of integrated whole-body PET/CT in the detection of recurrent ovarian cancer. *Eur J Radiol* **56**, 263–268.

[26] Makhija S, Howden N, Edwards R, Kelley J, Townsend DW, and Meltzer CC (2002). Positron emission tomography/computed tomography imaging for the detection of recurrent ovarian and fallopian tube carcinoma: a retrospective review. *Gynecol Oncol* **85**, 53–58.

[27] Sebastian S, Lee SI, Horowitz NS, Scott JA, Fischman AJ, Simeone JF, Fuller AF, and Hahn PF (2008). PET-CT vs. CT alone in ovarian cancer recurrence. *Abdom Imaging* **33**, 112–118.

[28] Picchio M, Sironi S, Messa C, Mangili G, Landoni C, Gianolli L, Zangheri B, Vigano R, Aletti G, De Maarzi P, et al. (2003). Advanced ovarian carcinoma: usefulness of [(18)F]FDG-PET in combination with CT for lesion detection after primary treatment. *Q J Nucl Med* **47**, 77–84.

[29] Bristow RE, del Carmen MG, Pannu HK, Cohade C, Zahurak ML, Fishman EK, Wahl RL, and Montz FJ (2003). Clinically occult recurrent ovarian cancer: patient selection for secondary cytoreductive surgery using combined PET/CT. *Gynecol Oncol* **90**, 519–528.